Supporting information for the paper:

From organic ligand to metal−organic coordination polymer, and to metal−organic coordination polymer−cocrystal composite: a continuous promotion of proton conductivity of crystalline materials

Xiaoqiang Liang,* [a] Tingting Cao, Li Wang, [a] Changzheng Zheng, [a] Yamei Zhao, [a] Feng Zhang,* [c] Chen Wen, [b] Lei Feng [b] and Chengan Wan [b]

[a] *School of Environmental and Chemical Engineering, Xi'an Polytechnic University, Xi'an 710048, PR China, Email: xq-liang@163.com*

[b] *Beijing Spacecrafts, Beijing 100094, PR China*

[c] *Key Laboratory of Photochemical Biomaterials and Energy Storage Materials, Heilongjiang Province and College of Chemistry and Chemical Engineering, Harbin Normal University, Harbin 150025, PR China, Email: zhangfeng@hrbnu.edu.cn*

Table of Contents

Table S1 Selected bond lengths (Å) and angles (°) for compounds **1**−**3**.

		1	
N(1)−C(6)	1.335(3)	N(1)−C(9)	1.341(3)
N(2)−C(8)	1.317(3)	N(2)−C(9)	1.347(3)
N(3)−C(9)	1.336(3)	N(4)−C(2)	1.329(4)
N(4)−C(3)	1.329(4)	C(1)−C(2)	1.361(4)
C(1)−C(5)	1.379(4)	C(3)−C(4)	1.380(4)
C(4)−C(5)	1.386(4)	C(4)−C(6)	1.480(4)
C(6)−C(7)	1.374(4)	C(7)−C(8)	1.375(4)
N(1)−C(6)−C(4)	116.7(2)	N(1)−C(6)−C(7)	122.1(2)
N(1)−C(9)−N(2)	125.2(2)	N(1)−C(9)−N(3)	118.1(2)
N(2)−C(9)−N(3)	116.7(2)	N(2)−C(8)−C(7)	123.9(3)
N(4)−C(3)−C(4)	124.4(2)	N(4)−C(2)−C(1)	123.8(3)
C(1)−C(5)−C(4)	118.8(2)	C(2)−N(4)−C(3)	116.7(2)
C(2)−C(1)−C(5)	119.0(3)	C(3)−C(4)−C(6)	120.1(2)
C(3)−C(4)−C(5)	117.3(2)	C(4)−C(6)−C(7)	121.2(2)
C(5)−C(4)−C(6)	122.6(2)	C(6)−C(7)−C(8)	116.3(2)
C(6)−N(1)−C(9)	116.8(2)	C(8)−N(2)−C(9)	115.7(2)
		2	
Cu(1)−I(1)	2.810(5)	Cu1−I(1a)	2.628(5)
Cu(1)−N(1)	2.050(8)	Cu(1)−N(4a)	2.028(8)
I(1)−Cu(1)−N(1)	103.2(2)	I(1)−Cu(1)−N(4a)	100.7(2)
I(1)−Cu(1)−I(1a)	103.99(6)	N(1)−Cu(1)−N(4a)	116.3(3)
I(1a)−Cu(1)−N(1)	117.2(2)	N(4a)−Cu(1)− I(1a)	112.5(2)
Cu(1)−I(1)−Cu(1a)	76.01(6)		
		3	
Co(1)−O(1)	2.071(3)	Co(1)−O(1a)	2.071(3)
Co(1)−O(3)	2.133(4)	Co(1)−O(3a)	2.133(4)
Co(1)−N(1)	2.160(3)	Co(1)−N(1a)	2.160(3)
O(1)−Co(1)−O(3)	91.22(12)	O(1)−Co(1)−N(1)	91.11(11)
O(1)−Co(1)−O(1a)	180.00	O(1)−Co(1)−O(3a)	88.78(12)
O(1)−Co(1)−N(1a)	88.89(11)	O(3)−Co(1)−N(1)	91.67(11)
O(1a)−Co(1)−O(3a)	88.78(12)	O(3)−Co(1)−O(3a)	180.00
O(3)−Co(1)−N(1a)	88.33(11)	O(1a)−Co(1)−N(1)	88.89(11)
O(3a)−Co(1)−N(1)	88.33(11)	N(1)−Co(1)−N(1a)	180.00
O(1a)−Co(1)−O(3a)	91.22(12)	O(1a)−Co(1)−N(1a)	91.11(11)
O(3a)−Co(1)−N(1a)	91.67(11)		

Symmetry codes : a) 1−*x*, 1−*y*, 1−*z* for **2**; a) −*x*, 2−*y*, 2−*z* for **3**.

Table S2 Hydrogen−bonding geometry parameters (Å, °) for compounds **1**−**3**.

D−H···A	d(D−H)	d(H···A)	d(D···A)	∠(DHA)
		1		
N(3)−H(3A)···N(2a)	0.86	2.16	3.004(4)	167
N(3)−H(3B)···N(1b)	0.86	2.25	3.100(5)	172
		2		
N(2)−H(2B)···N(3a)	0.86	2.36	3.115(13)	146
		3		
O(3)−H(3A)···O(2)	0.93	1.97	2.696(5)	133
O(3)−H(3B)···O(8)	0.93	1.34	2.269(4)	178
O(3)−H(3B)···N(5a)	0.93	2.32	2.863(5)	117
N(4)−H(4A)···O(7)	0.86	1.96	2.811(6)	170
N(4)−H(4B)···O(4a)	0.86	2.15	2.919(5)	149
O(5)−H(5A)···N(8a)	0.82	1.96	2.767(5)	169
O(6)−H(6)···N(3)	0.82	1.88	2.692(5)	170
N(7)−H(7A)···O(7)	0.86	2.16	2.920(5)	147
N(7)−H(7B)···O(4a)	0.86	2.00	2.855(6)	170
O(8)−H(8A)···O(1b)	0.96	2.37	3.209(4)	145
O(8)−H(8B)···O(3c)	0.96	1.61	2.269(4)	122

Symmetry codes : a) $-x$, $1/2+y$, $1/2-z$; b) $-x$, $-1/2+y$, $1/2-z$ for **1**; a) $1-x$, $1-y$, $-z$ for **2**; a) $1-x$, $1-y$, $1-z$; b) $-x$, $2-y$, $2-z$; $1-x$, $2-y$, $2-z$ for **3**.

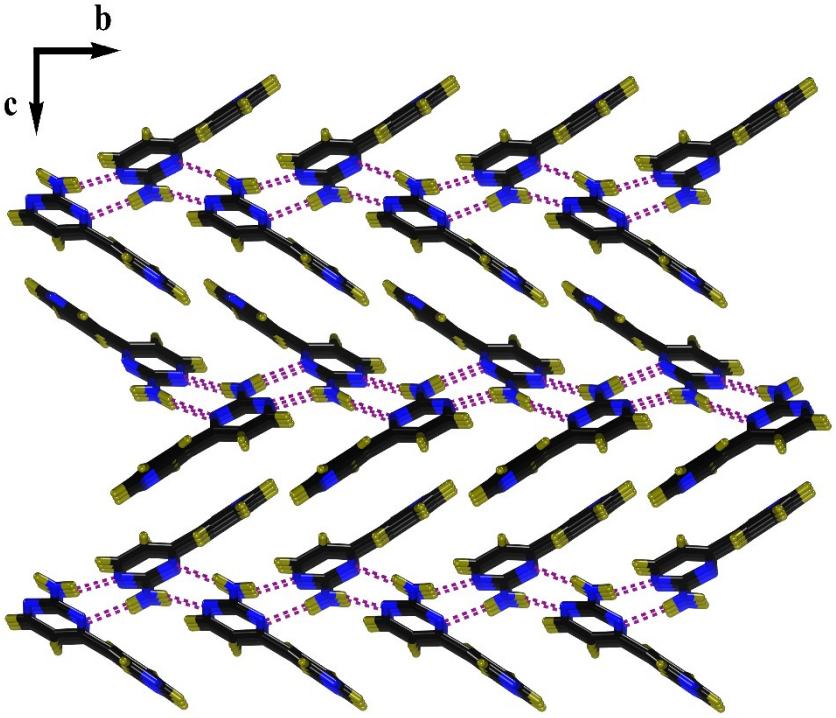

Fig. S1 The packing diagram of compound **1**. Pyridinic rings of other side gather with a head−to−head contact to form a hydrophobic area in the packing diagram. The alternately hydrophobic and hydrophilic (or hydrogen−bonding) areas is beneficial to stabilizing the solid−state structure (black, C; blue, N; dark green, H).

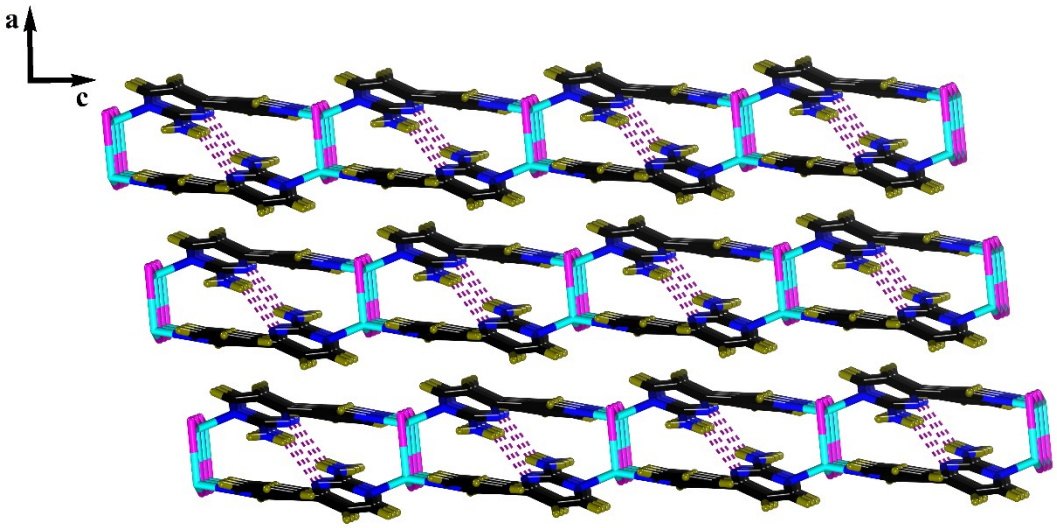

Fig. S2 The packing diagram of compound **2**. In the crystal packing diagram, the 2D layer repeat in an AA stacking sequence to generate hydrophilic−hydrophilic interaction, which can consolidate the crystal structure. (black, C; blue, N; cyan, Cu;

magenta, I; dark green, H).

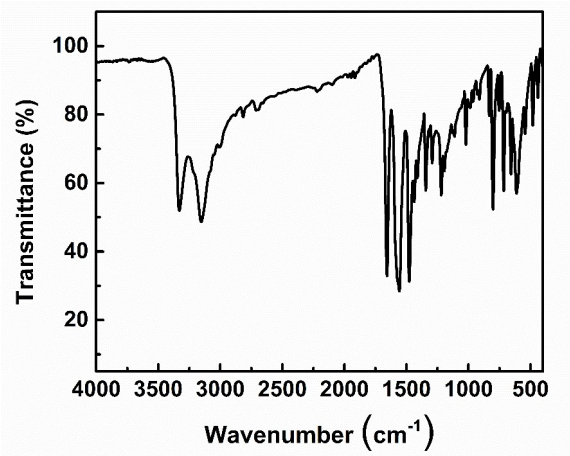

Fig. S3 IR absorption spectrum of compound **1** in the solid state at room temperature.

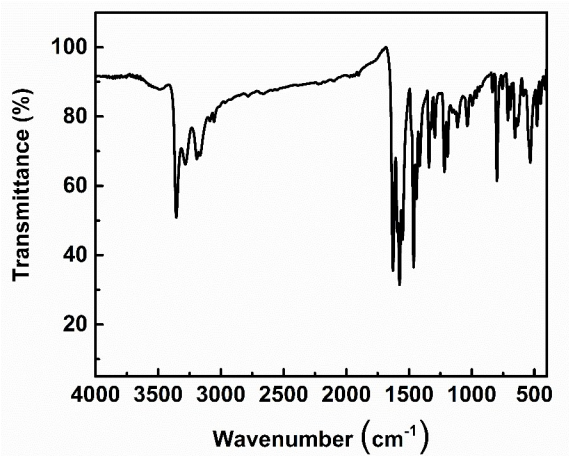

Fig. S4 IR absorption spectrum of compound **2** in the solid state at room temperature.

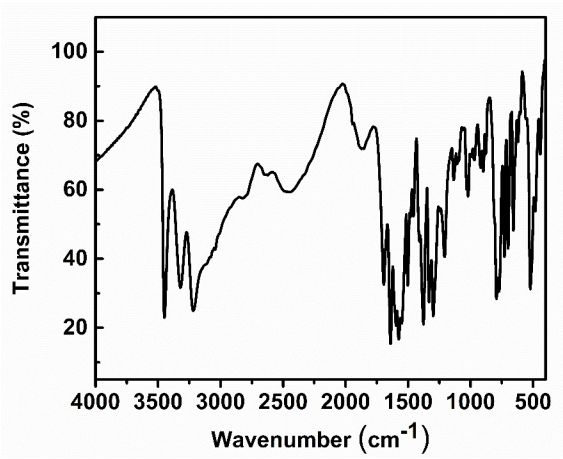

Fig. S5 IR absorption spectrum of compound **3** in the solid state at room temperature.

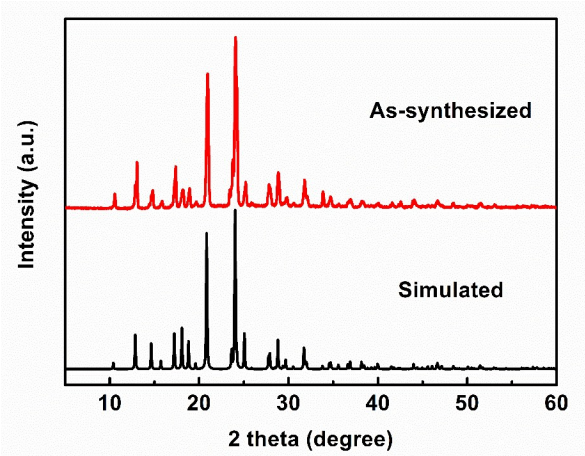

Fig. S6 The PXRD patterns for compound **1** of a simulation based on single−crystal analysis and as−synthesized bulk crystals.

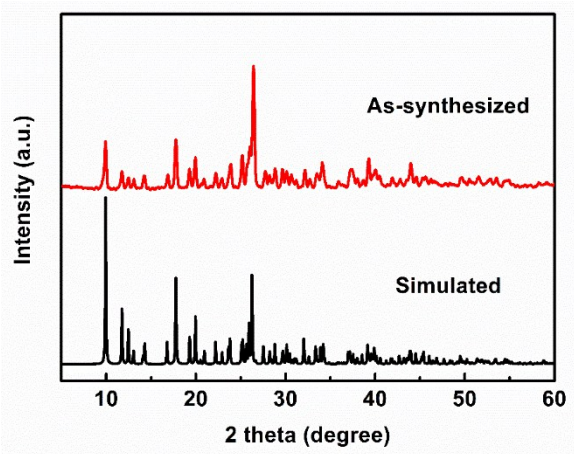

Fig. S7 The PXRD patterns for compound **2** of a simulation based on single−crystal analysis and as−synthesized bulk crystals.

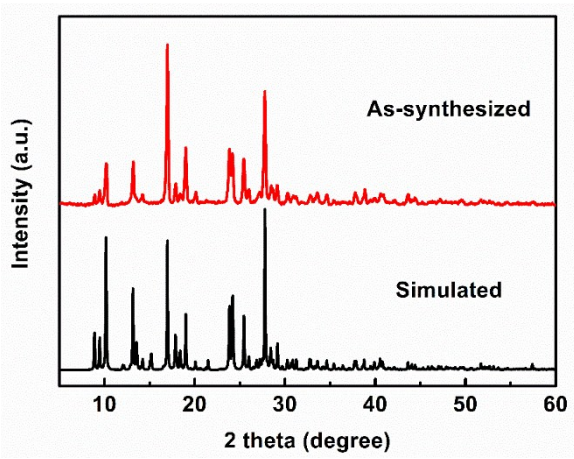

Fig. S8 The PXRD patterns for compound **3** of a simulation based on single−crystal

analysis and as−synthesized bulk crystals.

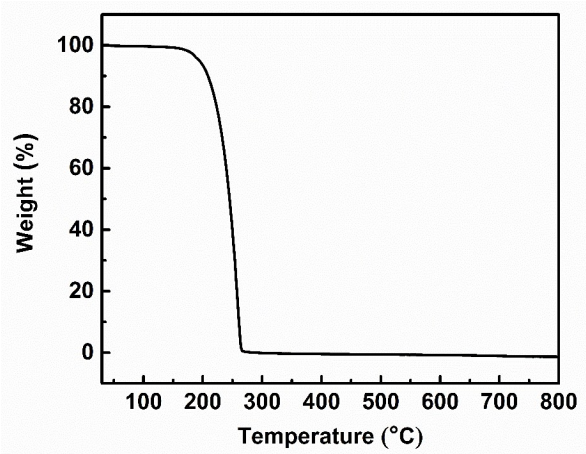

Fig. S9 Thermogravimetric curve for compound **1**.

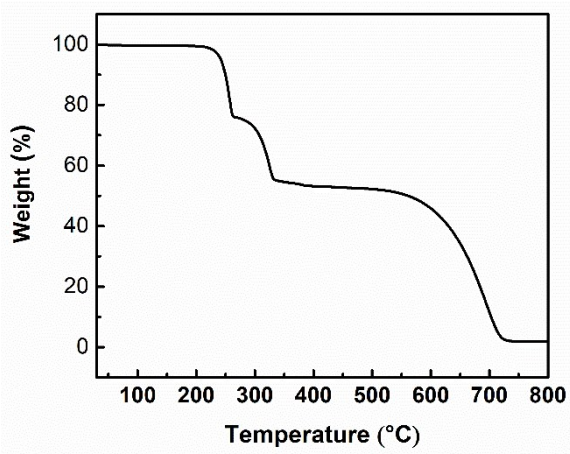

Fig. S10 Thermogravimetric curve for compound **2**.

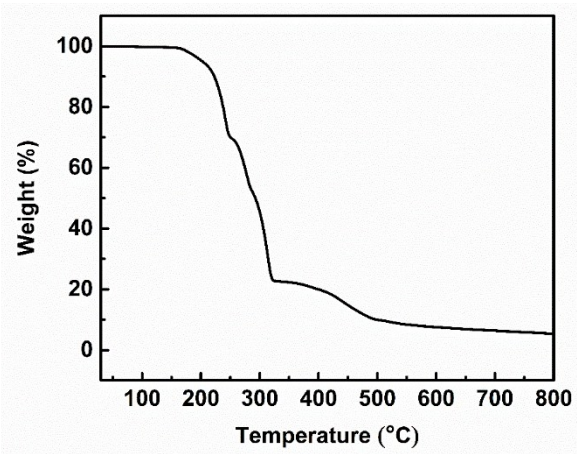

Fig. S11 Thermogravimetric curve for compound **3**.

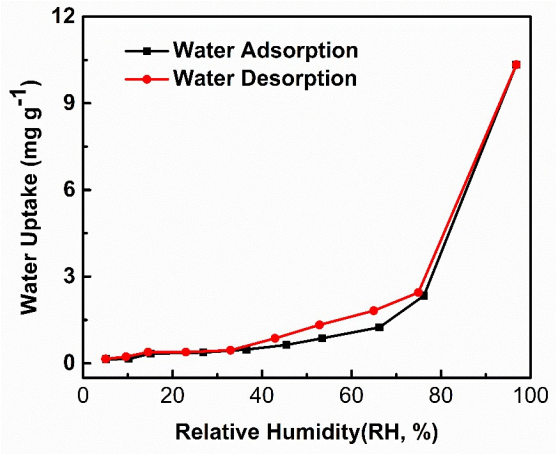

Fig. S12 Water adsorption–desorption isotherms of compound **1** at 298 K.

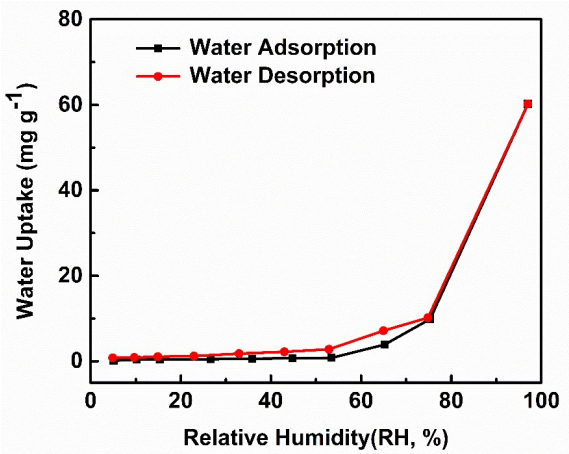

Fig. S13 Water adsorption–desorption isotherms of compound **2** at 298 K.

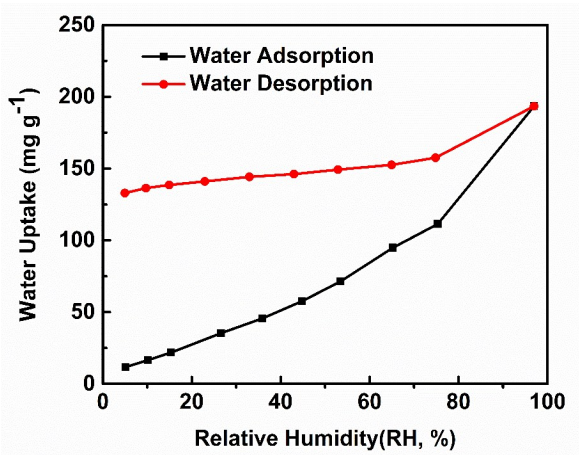

Fig. S14 Water adsorption–desorption isotherms of compound **3** at 298 K.

Analysis and Simulation of Impedance Plots:

The impedance plots consisting of a single semicircular arc at high frequency and a spike at low frequency are observed under higher RH conditions for compounds1−3. The high frequency arc may result from the bulk phase resistance and the low frequency resistance can be related to grain boundary resistance. On the contrary, there is an incomplete arc without the straight line lower high RH conditions for compounds 1−3, indicating a high bulk phase resistance. In view of powder samples, different equivalent circuits were selected to fit their Nyquist plots measured at different temperature and RH by ZSimpWin software. The equivalent circuit can match well with the measured impedance plots, which gives a lower value of chi−square, indicating that a good equivalent circuit. In ZSimpWin software, some principle elements, such as resistors (R), capacitors (C), constant phase element (CPE), inductors (L) and warburg diffusion element (W) can be usually used to fit the Nyquist plots. The equivalent circuit is shown in Scheme S1– S15. The relevant fits are illustrated in Fig. S15–S20.

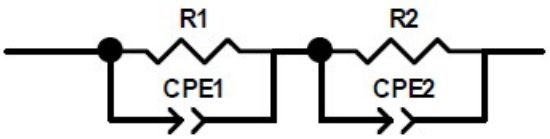

Scheme S1 The equivalent circuit (R_1CPE_1)(R_2CPE_2), which is suitable for the Nyquist plots of compound **1** at ~97% RH and 298K, 301K, 305K, 308K, 320K and 325K.

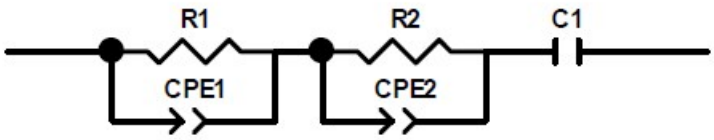

Scheme S2 The equivalent circuit (R_1CPE_1)(R_2CPE_2)C_1, which is suitable for the Nyquist plot of compound **1** at ~97% RH and 315 K.

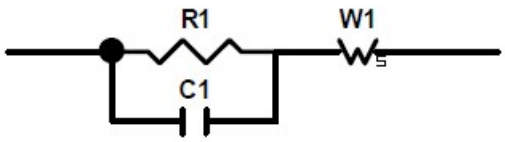

Scheme S3 The equivalent circuit (R_1C_1)W_1, which is suitable for the Nyquist plot of compound **1** at ~75% RH and 315 K.

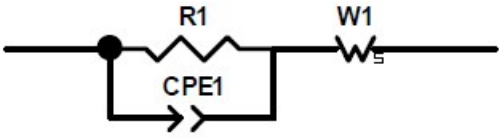

Scheme S4 The equivalent circuit (R_1CPE_1)W_1, which is suitable for the Nyquist plots of compound **1** at ~65% RH and 298 K, as well as compound **3** ~53% RH and 298 K.

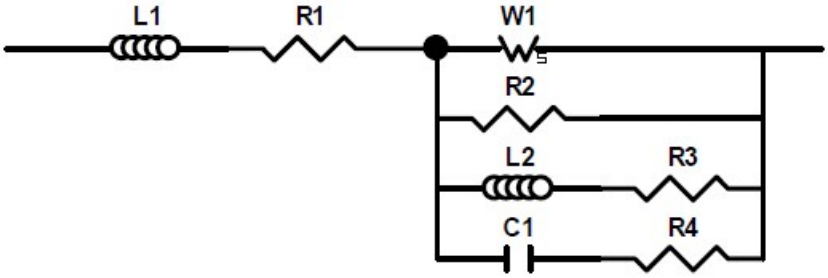

Scheme S5 The equivalent circuit $L_1R_1(W_1R_2(L_2R_3)(C_1R_4))$, which diffusion element, L_2 is the sample inductor, C_1 is a capacitor. The equivalent circuit is suitable for the Nyquist plot of compound **1** at ~53% RH and 315 K.

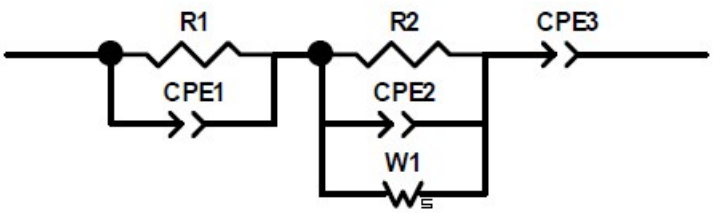

Scheme S6 The equivalent circuit (R_1CPE_1)($R_2CPE_2W_1$)CPE_3, which is suitable for the Nyquist plots of compound **2** at ~97% RH and 298K and 307 K.

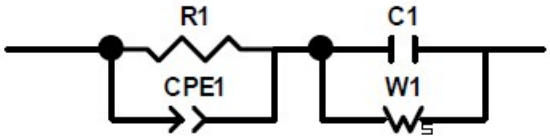

Scheme S7 The equivalent circuit (R_1CPE_1)(C_1W_1), which is suitable for the Nyquist plot of compound **2** at ~75% RH and 298K.

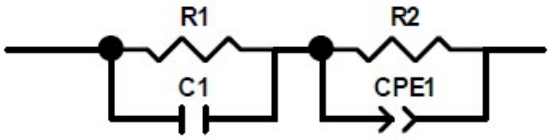

Scheme S8 The equivalent circuit (R_1C_1)(R_2CPE_1), which is suitable for the Nyquist plot of compound **2** at ~65% RH and 298K.

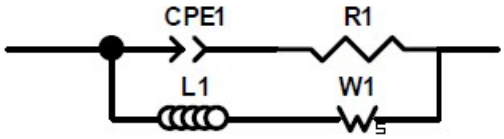

Scheme S9 The equivalent circuit (CPE_1R_1)(R_1W_1), which is suitable for the Nyquist plot of compound **2** at ~53% RH and 298K.

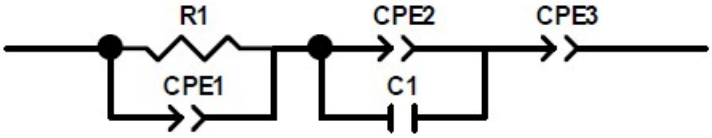

Scheme S10 The equivalent circuit (R_1CPE_1)(CPE_2C_1)CPE_3**,** which is suitable for the Nyquist plots of compound **2** at ~97% RH and 302 K and 317 K.

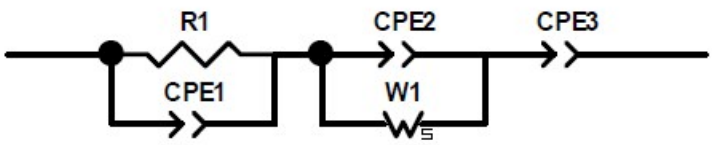

Scheme S11 The equivalent circuit $(R_1CPE_1)(CPE_2W_1)CPE_3$**,** which is suitable for the Nyquist plot of compound **2** at ~97% RH and 312 K.

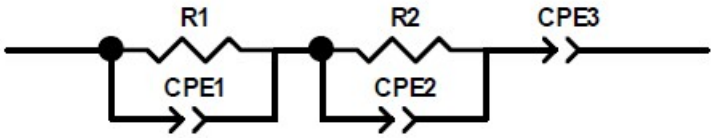

Scheme S12 The equivalent circuit $(R_1CPE_1)(R_2CPE_2)CPE_3$**,** which is suitable for the Nyquist plots of compound **2** at ~97% RH and 321 K and 325 K, as well as compound **3** at ~97% RH and 298K, 301K, 305K, 308K, 313K and 325 K.

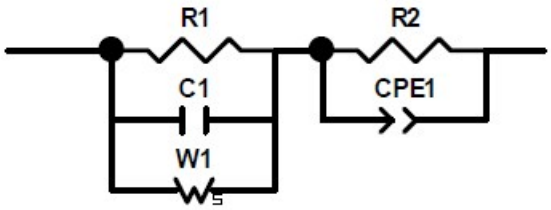

Scheme S13 The equivalent circuit $(R_1C_1W_1)(R_2CPE_1)$**,** which is suitable for the Nyquist plots of compound **3** at ~75% RH and 298 K.

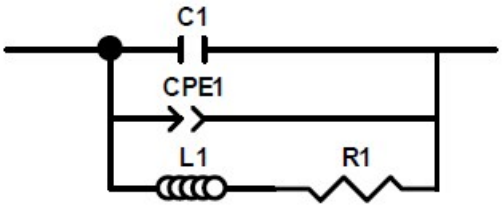

Scheme S14 The equivalent circuit $(C_1CPE_1(L_1R_1))$**,** which is suitable for the Nyquist plots of compound **3** at ~65% RH and 298 K.

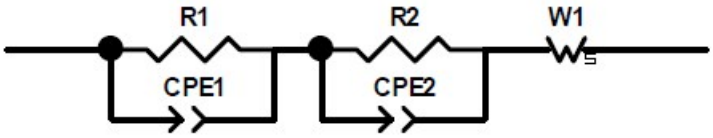

Scheme S15 The equivalent circuit $(R_1CPE_1)(R_2CPE_2)W_1$**,** which is suitable for the Nyquist plots of compound **3** at ~97% RH and 319 K.

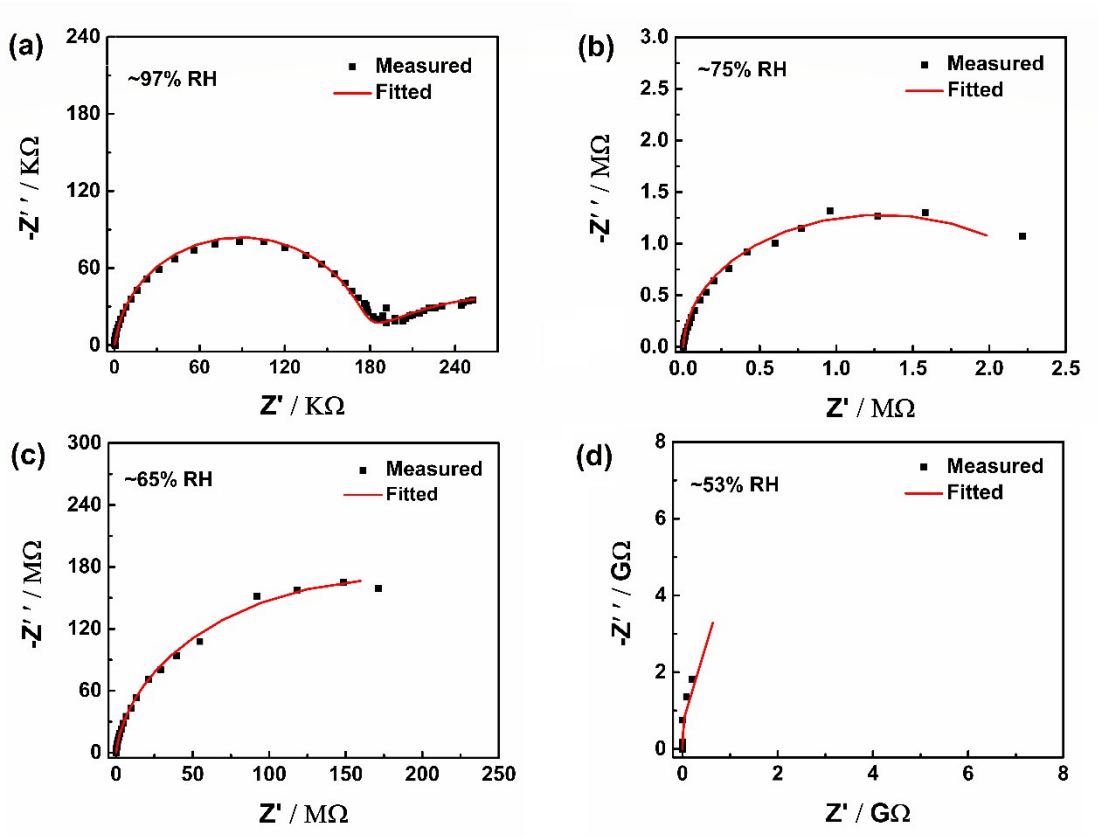

Fig. S15 Nyquist plots of compound **1** at different RH (relative humidity) and 298 K.

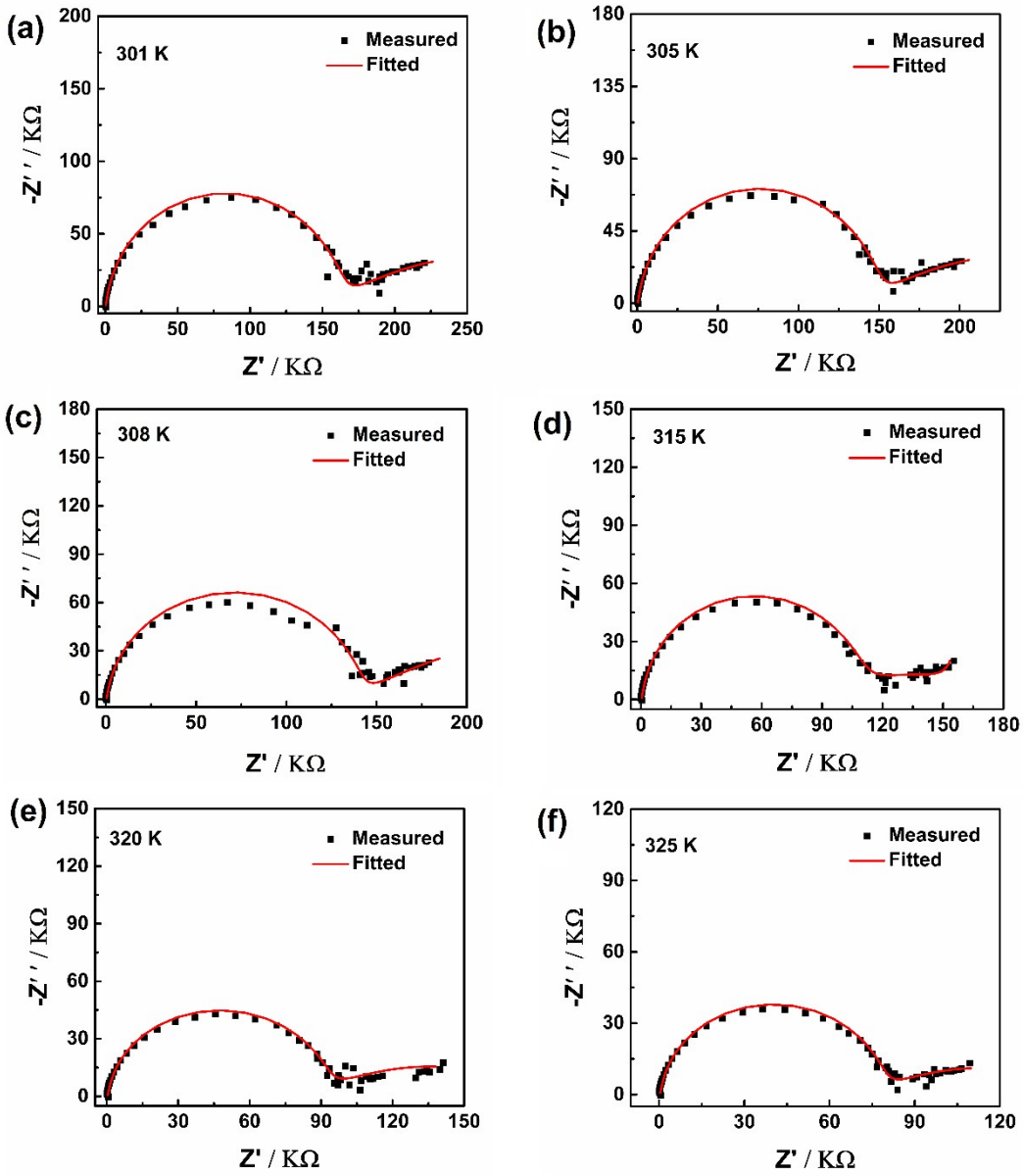

Fig. S16 Nyquist plots of compound **1** at different temperatures and ~97% RH (relative humidity).

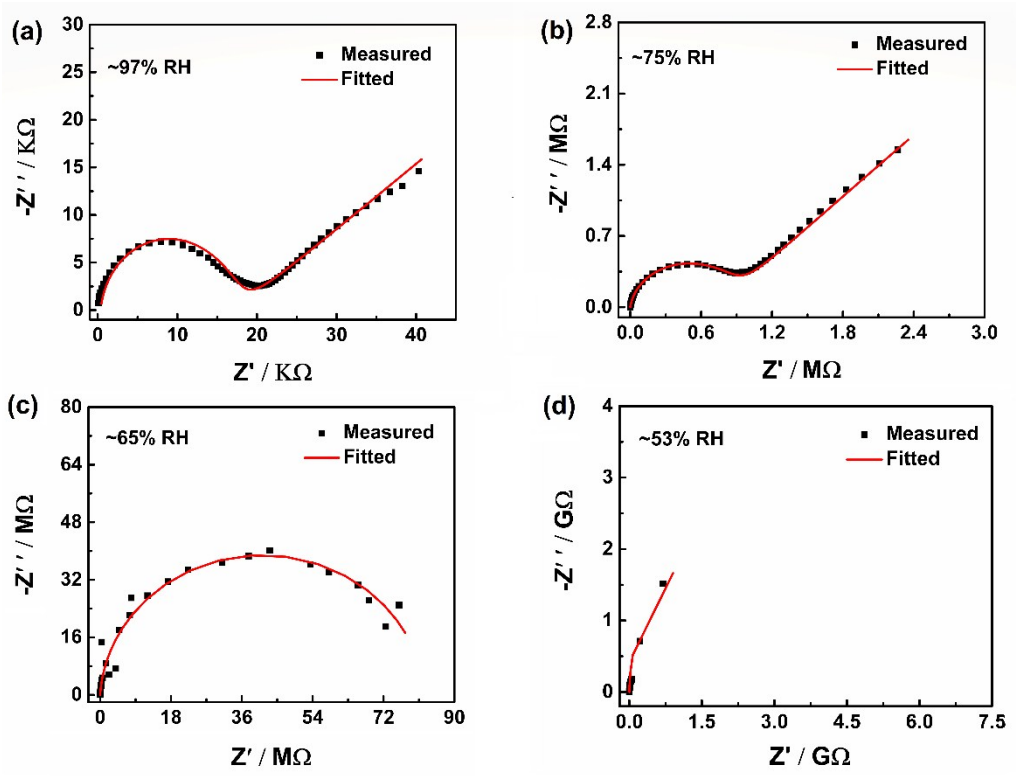

Fig. S17 Nyquist plots of compound **2** at different RH (relative humidity) and 298 K.

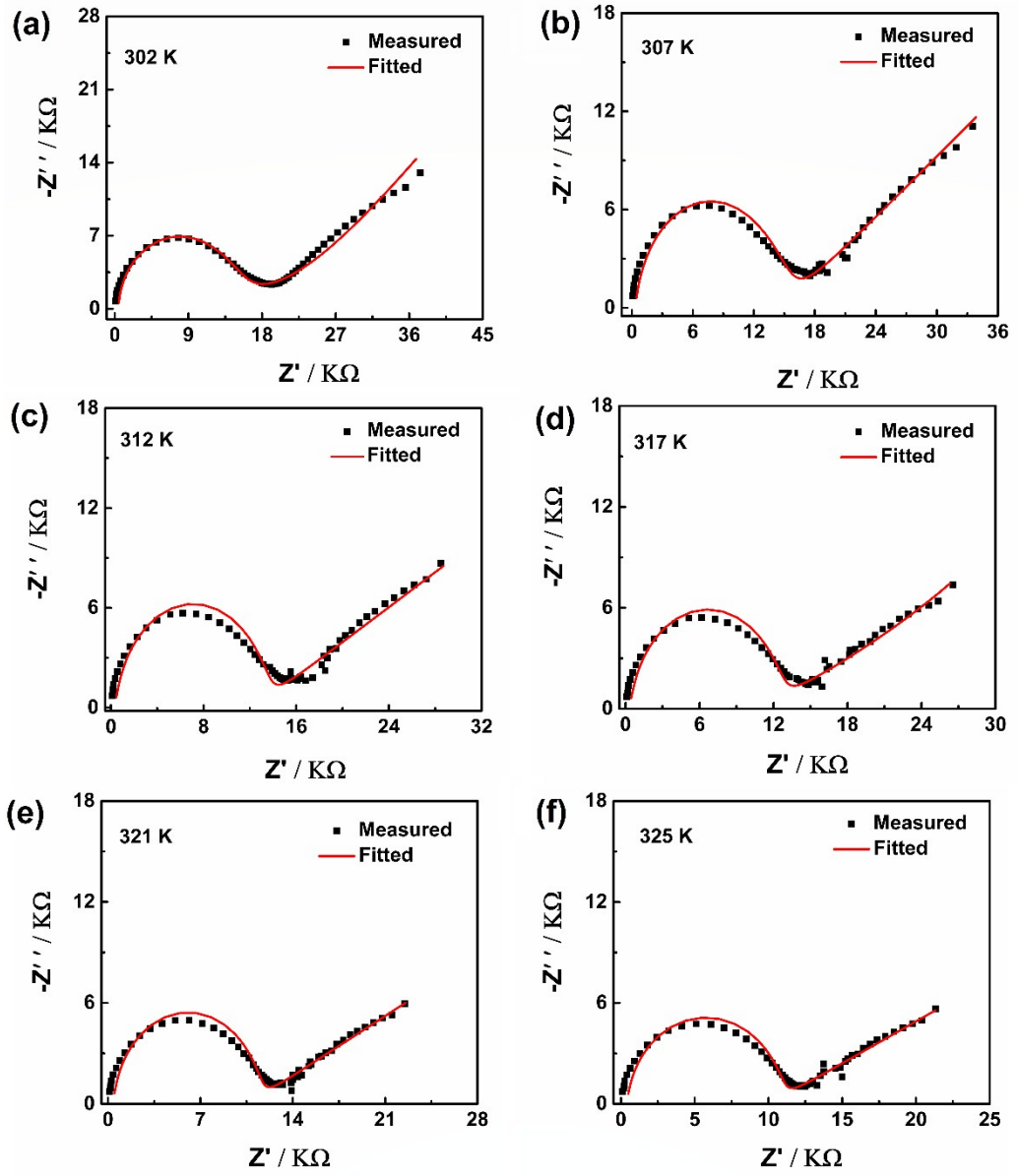

Fig. S18 Nyquist plots of compound **2** at different temperatures and ~97% RH (relative humidity).

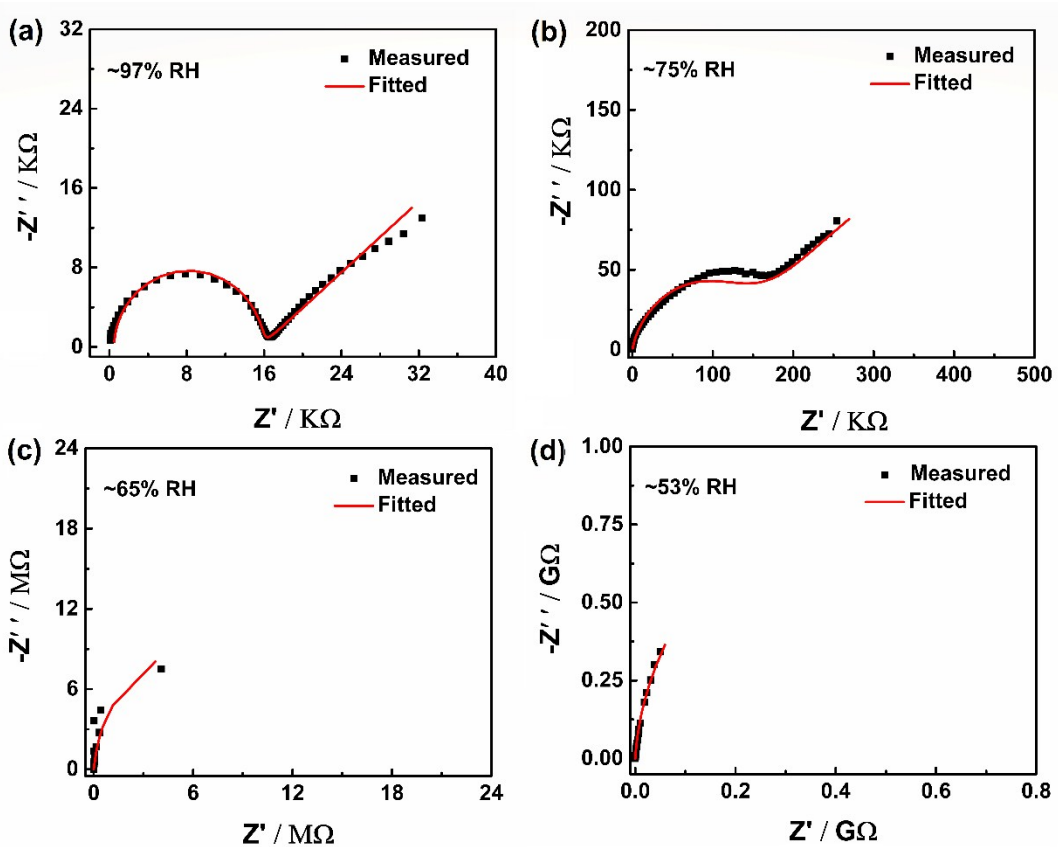

Fig. S19 Nyquist plots of compound **3** at different RH (relative humidity) and 298 K.

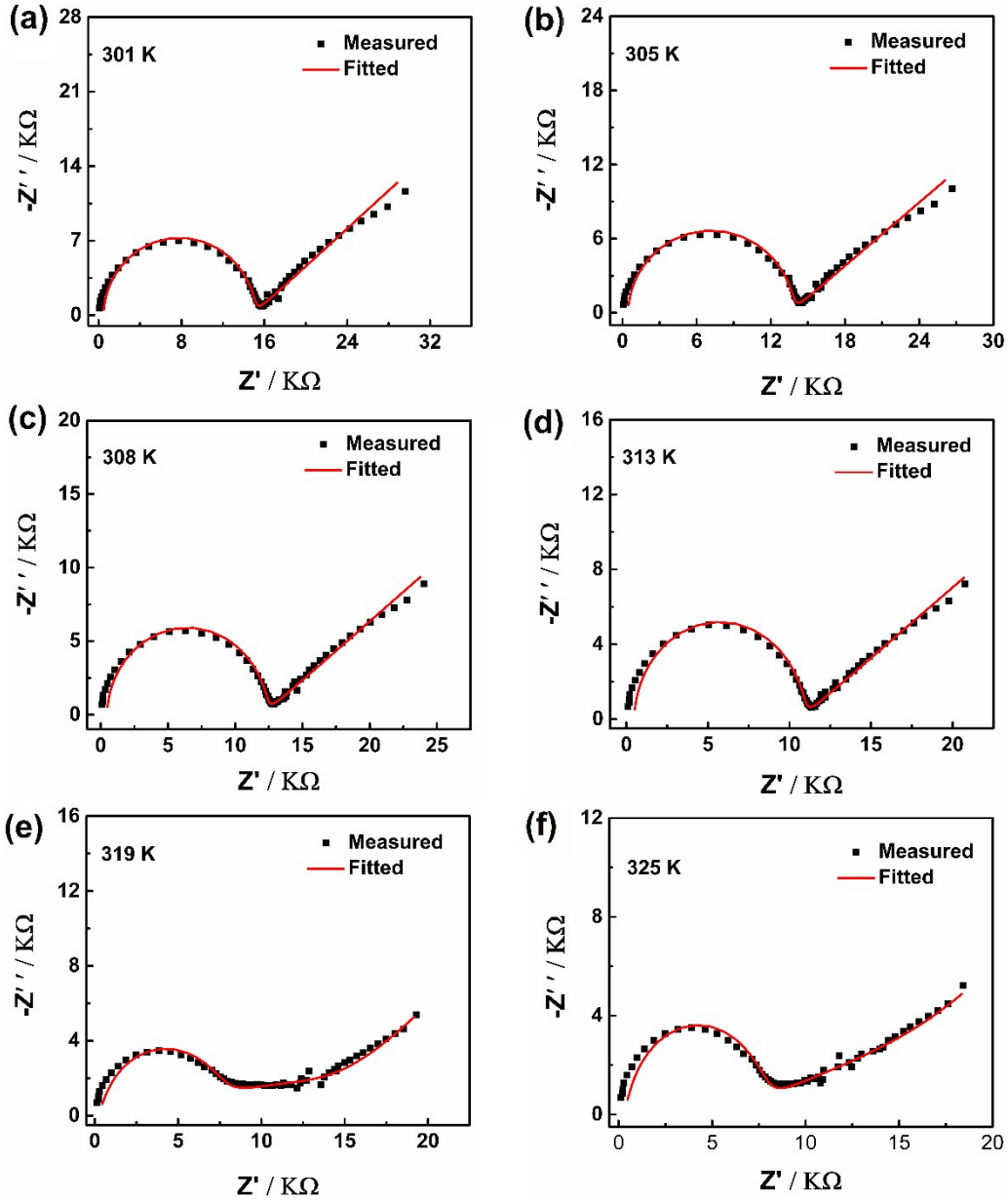

Fig. S20 Nyquist plots of compound **3** at different temperatures and ~97% RH (relative humidity).

Table S3 Comparison of proton conductivity of compound **3** with some reported proton conductors.

Materials	Proton Conductivity (S/cm)	Activation Energy (eV)	Temperature (K)	RH (%)	References
Compound 3	2.29×10^{-4}	0.24	325	~97	This Work
	1.20×10^{-4}		298		
$Zn_3(L)(H_2O)\cdot2H_2O$ [a]	3.5×10^{-5}	0.17	298	98	1
$Zn(l\text{-}L_{Cl})(Cl)\cdot2H_2O$ [b]	4.45×10^{-5}	0.34	298	98	2
$(H_2L2)_{0.5}[(Cu^{I}L2)_2(PMo_{12}O_{40})]\cdot H_2O$ [c]	1.9×10^{-4}	0.43	338	95	3
$\{[Zn\text{-}(C_{10}H_2O_8)_{0.5}(C_{10}S_2N_2H_8)]\cdot2H_2O]\}_n$ [d]	1.33×10^{-7}	0.84	298	95	4
$Co_2(H_2PO_3)_2(C_2O_4)_2(C_6N_2H_{16})$ [e]	8.43×10^{-7}	–	333	98	5
$Mn(C_2O_4)(C_{12}H_{14}N_6O_2)$ [f]	1.1×10^{-4}	0.41	298	98	6
$[Bi_4(HAzoBTC)_2(AzoBTC)(OH)_2(H_2O)_4]\cdot7H_2O$ [g]	1.0×10^{-4}	–	353	80	7
UMOM-100-b [h]	2.11×10^{-4}	0.66	353	90	8
$[Cu_4(S,S\text{ or }R,R\text{-}LOH)_3(NO_3)\cdot3H_2O]_n$ [i]	0.64×10^{-4}	0.34	298	97	9
(R)-$[Ni(pemp)(H_2O)_2]$ [j]	1.61×10^{-4}	0.24	298	95	10
$\{[Cu(H_2L)(H_2O)_2]_2[PW_{12}O_{40}]\}\{[Cu(HL)(H_2O)_2]_2[PW_{12}O_{40}]\}\cdot4CH_3OH\cdot4H_2O$ [k]	1.05×10^{-4}	0.16	298	98	11
$(NH_4)_2[Ag_4(mel)(NH_3)_2]\cdot3H_2O$ [l]	4.3×10^{-5}	0.47	358	98	12
$\{[Cd\text{-}(bpe)_{0.5}(5\text{-}sip)(H_2O)]\cdot4H_2O(bpeH_2)_{0.5}\}_n$ [m]	3.7×10^{-5}	0.37	335	95	13
Mg-BPTC [n]	2.60×10^{-4}	0.47, 1.18	373	98	14
$\{[Co_3(p\text{-}ClPhHIDC)_3(H_2O)_3]\cdot6H_2O\}_n$ [o]	2.47×10^{-4}	0.20	363	93	15
$Co(m\text{-}BrPhIDC)_2(H_2O)_6]\cdot2H_2O$ [p]	0.76×10^{-4}	0.56	373	98	16
$\{[Eu_3(bpydb)_3(HCOO)(OH)_2(DMF)]\cdot3DMF\cdot xH_2O\}_n$ [q]	1.7×10^{-4}	0.63	325	98	17

$\{[Er_3(pmpc)(C_2O_4)_3(H_2O)_7]\cdot 2H_2O\}_n$ [r]	8.1×10^{-5}	0.33	298	~97	18
$\{[Cu^I_3Cu^{II}_3L_3(DMF)_2(CH_3OH)(H_2O)]\cdot 3CH_3OH\}_n$ [s]	1.18×10^{-6}	0.63	303	98	19
HOF-H_3L [s]	1.12×10^{-6}	0.68	303	98	19
HOF-6a [t]	3.4×10^{-6}	–	300	~97	20
PA@Tp-Stb [u]	2.3×10^{-5}	–	332	98	21
$(H_{12}RCC1)^{12+}\cdot 6(SO_4)^{2-}\cdot 27.25(H_2O)$ [v]	6.1×10^{-5}	0.10	303	95	22
$CB[8]\cdot 6.8HCO_2H\cdot 13H_2O$ [w]	1.3×10^{-4}	0.56	298	98	23
$[(H_3betc)(H\text{-}Hopip)_{0.5}\cdot(H_2O)]$ [x]	1.34×10^{-4}	0.41	298	~97	24
GINZH [y]	1.1×10^{-4}	0.20	307	98	25
GISH [z]	2.0×10^{-4}	0.39	293	98	26

[a] L = $[1,3,5\text{-benzenetriphosphonate}]^{6-}$. [b] l-$L_{Cl}$ = N-(4-pyridylmethyl)-L-valine·HCl. [c] L2 = 1,4-bis((1H-1,2,4-triazol-1-yl)methyl)-benzene. [d] $C_{10}H_2O_8$ = pyromellitate, $C_{10}S_2N_2H_8$ = 4-pyridinethiolate. [e] $H_2C_2O_4$ = oxalic acid, and $C_6H_{14}N_2$ = cis-2,6-dimethylpiperazine. [f] $C_{12}H_{14}N_6O_2$ = cyclic dipeptides generated by racemic histidine molecules. [g] H_4AzoBTC = 3,3′,5,5′-azobenzenetetracarboxylic acid. [h] UMOM-100-b = the incorporation of acid functionalized Cu(II)-based nanosized cuboctahedron MOP into a mesoporous MOF, PCN-777. [i] S,S or R,R-LOH = (S,S or R,R)-3,5-bis-(1-hydroxyethyl)-1,2,4-triazolate). [j] $pemp^{2-}$ = (R)- (1-phenylethylamino)-methylphosphonate. [k] H_2L = 4,4′-bis(hydroxymethyl)-2,2′-bipyridine. [l] mel = $[\text{benzenehexacarboxylate}]^{6-}$. [m] 5-sip = tri-negative 5-sulfoisophthalate salt, bpe = 4,4′-bispyridylethane. [n] H_4BPTC = 2,2',6,6'- tetracarboxybiphenyl. [o] *p*-$ClPhH_3IDC$ = 2-(p-chloro -phenyl)-imidazole-4,5-dicarboxylic acid. [p] *o*-$BrPhH_3IDC$ = 2-(o-bromo-phenyl)-imidazole-4,5-dicarboxylic acid. [q] $bpydbH_2$ = 4,4′-(4,4′-bipyridine-2,6-diyl) dibenzoic acid, DMF = *N*,*N*′-dimethyl -formamide. [r] H_3pmpc = 1-(phosphonomethyl)piperidine-3-carboxylic acid. [s] H_3L = [3-(4-methyl-benzoyl)-thioureido]-acetic acid. [t] HOF 6a = an activate 5,10,15,20-tetrakis(4-(2,4-diaminotriazinyl)phenyl)-porphyrin. [u] PA = loaded H_3PO_4, Tp = triformylphloroglucinol, Stb = 4,4'-diaminostilbene. [v] H_{12}RCC1 = a porous organic cage material. [w] CB8 = cucurbit[8]uril. [x] H_4betc = 1,2,4,5-benzenetetracarboxylic acid, Hopip = homopiperazine. [y] GINZH = a gallic acid-isoniazid cocrystal compound. [z] GISH = a hydrated sulfuric salt of gallic acid and isoniazid.

References

1. J. M. Taylor, R. K. Mah, I. L. Moudrakovski, C. I. Ratcliffe, R. Vaidhyanathan and G. K. H. Shimizu, *J. Am. Chem. Soc.*, 2010, **132**, 14055.
2. S. C. Sahoo, T. Kundu and R. Banerjee, *J. Am. Chem. Soc.,* 2011, **133**, 17950.
3. K. Lu, A. L. Peláez, L. Wu, Y. Cao, C. Zhu, and H. Fu, *Inorg. Chem.*, 2019, **58**, 1794.
4. S. Sanda, S. Biswas and Sanjit Konar, *Inorg. Chem.*, 2015, **54**, 1218.
5. F. Gao, L. Huang, Z. Xiu, Y. Yin, Y. Ma, Y. Bi and Z. Zheng, *CrystEngComm*, 2018, **20**, 5544.
6. J. Shi, J. Li, H. Zeng, G. Zou, Q. Zhang and Z. Lin, *Dalton Trans.*, 2018, **47**, 15288.
7. S. M. F. Vilela, T. Devic, A. Várez, F. Salles and P. Horcajada, *Dalton Trans.*, 2019, **48**, 11181.
8. J. Lee, D. -W. Lim, S. Dekura, H. Kitagawa and W. Choe, *ACS Appl. Mater. Interfaces*, 2019, **11**, 12639.
9. B. Q. Song, D. Q. Chen, Z. Ji, J. Tang, X. L. Wang, H. Y. Zang and Z. M. Su, *Chem. Commun.*, 2017, **53**, 1892.
10. X. -G. Liu, S. -S. Bao, J. Huang, K. Otsubo, J. S. Feng, M. Ren, F. C. Hu, Z. Sun, L. M. Zheng, S. Wei and H. Kitagawa, *Chem. Commun.*, 2015, **51**, 15141.
11. H. Yang, X. Y. Duan, J. J. Lai, Y. Zhao, X. J. Wang and M. L. Wei, *Inorg. Chem.*, 2019, **58**, 446.
12. X. Y. Dong, X. Li, B. Li, Y. Y. Zhu, S. Q. Zang and M. S. Tang, *Dalton Trans.*, 2016, **45**, 18142.
13. D. K. Maity, S. Ghosh, K. Otake, H. Kitagawa and D. Ghoshal, *Inorg. Chem.*, 2019, **58**, 12943.
14. X. Y. Dong, X. P. Hu, H. C. Yao, S. Q. Zang, H. W. Hou and T. C. W. Mak, *Inorg. Chem.*, 2014, **53**, 12050.
15. X. Liang, B. Li, M. H. Wang, J. Wang, R. L. Liu, G. Li, *ACS Appl. Mater. Interfaces.*, 2017, **9**, 25082.
16. R. L. Liu, L. L. Zhao, W. Dai, C. L. Yang and G. Li, *Inorg. Chem.*, 2018, **57**, 1474.
17. S. L. Yang, P. P. Sun, Y. Y. Yuan, C. X. Zhang and Q. L. Wang, *CrystEngComm*, 2018, **20**, 3066.
18. X. Liang, K. Cai, F. Zhang, J. Liu and G. Zhu, *J. Mater. Chem. A***,** 2017, **5**, 25350.
19. Z. B. Sun, Y. L. Li, Z. H. Zhang, Z. F. Li, B. Xiao and G. Li, *New J. Chem.*, 2019, **43**, 10637.
20. W. Yang, F. Yang, T. L. Hu, S. C. King, H. L. Wang, H. Wu, W. Zhou, J. R. Li, H. D. A. Arman, B. L. Chen, *Cryst. Growth Des.*, 2016, **16**, 5831.
21. S. Chandra, T. Kundu, S. Kandambeth, R. BabaRao, Y. Marathe, S. M. Kunjir, and R. Banerjee, *J. Am. Chem. Soc.,* 2014, **136**, 6570.
22. M. Liu, L. Chen, S. Lewis, S. Y. Chong, M. A. Little, T. Hasell, I. M. Aldous, C.

M. Brown, M. W. Smith, C. A. Morrison, L. J. Hardwick and A. I. Cooper, *Nat. Comm.* 2016, **7**, 12750.
23. M. Yoon, K. Suh, H. Kim, Y. Kim, N. Selvapalam and K. Kim, *Angew. Chem., Int. Ed.*, 2011, **50**, 7870.
24. X. Liang, Y. Chen, L. Wang, F. Zhang, Z. Fan, T. Cao, Y. Cao, H. Zhu, X. He, B. Deng, Y. You, Y. Dong and Y. Zhao, *New J. Chem.*, 2019, **43**, 11099.
25. R. Kaur, B. Ponraj, D. Swain, K. B. R. Varma and T. N. G. Row, *Cryst. Growth Des.,* 2015, **15**, 4171.
26. R. Kaur, D. Swain, D. Dutta, K. Brajesh, P. Singh, A. J. Bhattacharyya, R. Ranjan, C. Narayana, J. Hulliger and T. N. G. Row, *J. Phys. Chem. C*, 2017, **121**, 18317.